Monthly Notices
of the
ROYAL ASTRONOMICAL SOCIETY

Mon. Not. R. Astron. Soc. **406,** 2650–2662 (2010) doi:10.1111/j.1365-2966.2010.16864.x

Electromagnetic counterparts of compact object mergers powered by the radioactive decay of *r*-process nuclei

B. D. Metzger,[1⋆†] G. Martínez-Pinedo,[2] S. Darbha,[3] E. Quataert,[3] A. Arcones,[2,4] D. Kasen,[5‡] R. Thomas,[6] P. Nugent,[6] I. V. Panov[7,8,9] and N. T. Zinner[10]

[1]*Department of Astrophysical Sciences, Princeton University, Princeton, NJ 08544, USA*
[2]*GSI Helmholtzzentrum für Schwerionenforschung, Planckstr. 1, D-64291 Darmstadt, Germany*
[3]*Astronomy Department and Theoretical Astrophysics Center, University of California, Berkeley, 601 Campbell Hall, Berkeley, CA 94720, USA*
[4]*Institut für Kernphysik, TU Darmstadt, Schlossgartenstr. 9, D-64289 Darmstadt, Germany*
[5]*University of California, Santa Cruz, CA 95064, USA*
[6]*Computational Cosmology Center, Lawrence Berkeley National Laboratory, 1 Cyclotron Road MS50B-4206, Berkeley, CA 94720, USA*
[7]*Department of Physics, University of Basel, Klingelbergstr. 82, CH-4056 Basel, Switzerland*
[8]*Institute for Theoretical and Experimental Physics, B. Cheremushkinskaya St. 25, 117259 Moscow, Russia*
[9]*Russian Research Centre Kurchatov Institute, pl. Kurchatova 1, 123182 Moscow, Russia*
[10]*Department of Physics, Harvard University, Cambridge, MA 02138, USA*

Accepted 2010 April 18. Received 2010 April 12; in original form 2010 January 28

ABSTRACT

The most promising astrophysical sources of kHz gravitational waves (GWs) are the inspiral and merger of binary neutron star(NS)/black hole systems. Maximizing the scientific return of a GW detection will require identifying a coincident electromagnetic (EM) counterpart. One of the most likely sources of *isotropic* EM emission from compact object mergers is a supernova-like transient powered by the radioactive decay of heavy elements synthesized in ejecta from the merger. We present the first calculations of the optical transients from compact object mergers that self-consistently determine the radioactive heating by means of a nuclear reaction network; using this heating rate, we model the light curve with a one-dimensional Monte Carlo radiation transfer calculation. For an ejecta mass $\sim 10^{-2}\,\mathrm{M}_\odot$ ($10^{-3}\,\mathrm{M}_\odot$) the resulting light-curve peaks on a time-scale $\sim$1 d at a V-band luminosity $\nu L_\nu \sim 3 \times 10^{41}$ (10^{41}) erg s^{-1} [$M_V = -15(-14)$]; this corresponds to an effective 'f' parameter $\sim 3 \times 10^{-6}$ in the Li–Paczynski toy model. We argue that these results are relatively insensitive to uncertainties in the relevant nuclear physics and to the precise early-time dynamics and ejecta composition. Since NS merger transients peak at a luminosity that is a factor of $\sim 10^3$ higher than a typical nova, we propose naming these events 'kilo-novae'. Because of the rapid evolution and low luminosity of NS merger transients, EM counterpart searches triggered by GW detections will require close collaboration between the GW and astronomical communities. NS merger transients may also be detectable following a short-duration gamma-ray burst or 'blindly' with present or upcoming optical transient surveys. Because the emission produced by NS merger ejecta is powered by the formation of rare *r*-process elements, current optical transient surveys can directly constrain the unknown origin of the heaviest elements in the Universe.

Key words: gravitation – nuclear reactions, nucleosynthesis, abundances – binaries: close – gamma-ray burst: general – stars: neutron – supernovae: general.

1 INTRODUCTION

The direct detection of gravitational waves (GWs) would be a major breakthrough for both fundamental physics and astrophysics. With upgrades of the ground-based interferometers LIGO (Abramovici et al. 1992) and Virgo (e.g. Caron et al. 1999) to 'advanced' sensitivity expected within the next decade, GW detection is rapidly becoming a realistic – even anticipated – possibility.

The most promising astrophysical sources of GWs for ground-based detectors are thought to be the GW-driven inspiral and coalescence of binary compact objects [neutron stars (NSs) and black holes (BHs)]. Advances in general relativistic simulations of the merger process (Pretorius 2005; Baker et al. 2006;

⋆E-mail: bmetzger@astro.princeton.edu
†NASA Einstein Fellow.
‡Hubbel Fellow.

Campanelli et al. 2006) are honing our understanding of the strength and form of the expected signal (see e.g. Duez 2009; Faber 2009, for recent reviews). However, estimates of the merger rates based on known NS–NS binaries and population synthesis remain uncertain by at least an order of magnitude (Kim et al. 2005; Belczynski et al. 2006; Kalogera et al. 2007; LIGO Scientific Collaboration & Virgo Collaboration 2010). For instance, Kim et al. (2005) estimate that the NS–NS merger rate detectable with advanced LIGO will be $27^{+62}_{-21}\,\mathrm{yr}^{-1}$, implying that if the true rate lies on the low end of present estimates then only a few sources may be detected per year. This possibility makes it especially crucial that we extract the most science from each event.

Optimizing the science from a detected GW signal requires identifying a coincident electromagnetic (EM) counterpart (e.g. Schutz 1986, 2002; Sylvestre 2003; Stubbs 2008; Bloom et al. 2009a; Phinney 2009; Stamatikos et al. 2009). By independently identifying the source's position and time, several of the degeneracies associated with the GW signal are lifted (Hughes & Holz 2003; Arun et al. 2009) and the signal-to-noise ratio required for a confident detection is decreased (Kochanek & Piran 1993; Dalal et al. 2006). Coupled with its GW-measured luminosity distance, identifying the merger's redshift (e.g. by localizing its host galaxy) would also allow for a precision measurement of the Hubble constant (e.g. Krolak & Schutz 1987; Holz & Hughes 2005; Deffayet & Menou 2007). Likewise, the potential wealth of complementary information encoded in the EM signal may be essential to fully unravelling the astrophysical context of the event (Phinney 2009).

The most commonly discussed EM signal associated with NS–NS/NS–BH mergers is a short-duration gamma-ray burst (GRB), powered by the accretion of material that remains in a centrifugally supported torus around the BH following the merger (Paczynski 1986; Narayan, Paczynski & Piran 1992). The *Swift* satellite (Gehrels et al. 2004) has revolutionized our understanding of short GRBs by detecting and localizing a significant number of their afterglows for the first time. This has enabled the discovery that short GRBs likely originate from a more evolved stellar population than those of long-duration GRBs (e.g. Berger et al. 2005; Villasenor et al. 2005; Bloom et al. 2006; see Berger 2009 for a recent review), consistent with an origin associated with compact object mergers (Nakar, Gal-Yam & Fox 2006). Despite these suggestive hints, however, it is not yet established that all short GRBs are uniquely associated with NS–NS/NS–BH mergers (e.g. Hurley et al. 2005; Metzger, Quataert & Thompson 2008a) nor that all mergers lead to an energetic GRB. Furthermore, only a small fraction of GRB jets are pointed towards us (Rhoads 1999) and for off-axis events, the prompt and afterglow emission are much dimmer due to relativistic debeaming. Although some emission may be observed by off-axis viewers, such 'orphan' afterglows (e.g. Totani & Panaitescu 2002) are typically expected to peak at radio wavelengths on a time-scale of months–years (Soderberg et al. 2006a; Rossi, Perna & Daigne 2008; Zhang & MacFadyen 2009). Only a limited fraction of short GRBs are detected in radio, even when viewed on-axis (e.g. Soderberg et al. 2006b).

In parallel to the advances in GW detectors, the advent of large-scale optical surveys with increasing sensitivity, rapid cadence and sky-area coverage is leading to a revolution in the study of transient objects. These include the Palomar Transient Factory (PTF; Rau et al. 2009), Pan-STARRs (Kaiser et al. 2002), SkyMapper (Keller et al. 2007) and the VLT Survey Telescope (VST; Mancini et al. 2000), which are paving the way for future endeavours such as the Large Synoptic Survey Telescope (LSST; Strauss et al. 2010) and the proposed Synoptic All Sky Infrared Imaging (SASIR) survey (Bloom et al. 2009b). Given these present and anticipated future capabilities, the most promising EM counterpart of compact object mergers is arguably an *isotropic*, *optical/near-infrared (NIR)* wavelength signal. In addition to providing time-stamped maps of the night sky for use in follow-up observations, these 'blind' surveys could also detect EM counterparts even independent of a GW or GRB trigger (see Section 5.3).

One proposed source of relatively isotropic optical/NIR emission following a NS–NS/NS–BH merger is a supernova (SN)-like transient powered by the radioactive decay of merger ejecta (Li & Paczyński 1998, hereafter LP98; cf. Kulkarni 2005; Metzger, Piro & Quataert 2008b). Although Type Ia supernova light curves are powered largely by the decay of ^{56}Ni (e.g. Kasen & Woosley 2009), most of the ejecta from NS–NS/NS–BH mergers is highly neutron rich (electron fraction $Y_\mathrm{e} \sim 0.1$–0.4) and produces little Ni. Instead, much heavier radioactive elements are formed via rapid neutron capture (r-process) nucleosynthesis following the decompression of the ejecta from nuclear densities (e.g. Lattimer & Schramm 1974, 1976; Eichler et al. 1989; Freiburghaus, Rosswog & Thielemann 1999). Although the r-process itself lasts only a matter of seconds, these newly synthesized elements undergo nuclear fission, alpha and beta decays on much longer time-scales as they descend to β-stability. The resulting energy release can power detectable thermal emission once the ejecta expands sufficiently that photons can escape. Because of the lower quantity of ejecta and its faster speed, however, the resulting transient is dimmer and evolves faster than a normal SN. Transients from NS mergers are thus a challenge to detect and identify.

Although the basic LP98 model provides a qualitative picture of the thermal transients from NS–NS/NS–BH mergers, it makes a number of simplifying assumptions and leaves several free parameters unconstrained, including the fraction of nuclear energy released and the precise distribution of decaying nuclei. LP98 further assume that the photosphere radiates as a blackbody, which is a poor assumption at moderate optical depths and in light of the substantial UV line blanketing that may accompany the rich energy spectra of the very heavy nuclei that dominate the composition. These details may be important for predicting the unique, 'smoking gun' features of merger-related transients. Because the transient sky is expected to be rich in its diversity (e.g. Becker et al. 2004), more detailed predictions may be essential to identifying candidate sources in real-time for deeper follow-up observations, especially considering the likelihood that only limited information (e.g. photometric colours) may be available. Understanding the detailed *spectroscopic* properties of merger transients is clearly an important endeavour.

In this work we present the first self-consistent calculations of the optical/NIR counterparts to NS–NS/NS–BH mergers. In particular, our work goes beyond previous work in two important ways: (1) we use a nuclear physics reaction network to calculate the radioactive heating of the ejecta and (2) we employ the Monte Carlo radiative transfer code SEDONA to more accurately model the light curve and colours of the resulting EM transient. We begin in Section 2 with preliminary considerations, including a discussion of the sources of neutron-rich ejecta from NS–NS/NS–BH mergers (Section 2.1) and a brief review of the relevant scalings for radioactively powered transients (Section 2.2). In Section 3 we describe the nucleosynthesis that occurs as the material decompresses from nuclear densities and our calculations of the resulting radioactive heating, including a detailed discussion of the efficiency of fission/β-decay thermalization (Section 3.2). In Section 4 we present calculations of the light curves and colour evolution of NS–NS/NS–BH merger transients, highlighting the unique features of these events and the

primary uncertainties in the theoretical predictions. We find that the peak luminosities of NS merger transients are typically $\sim$few $\times$ 10^{41} erg s^{-1}, or a factor of $\sim 10^3$ larger than the Eddington luminosity for a solar mass object. We therefore dub these events 'kilonovae', since standard novae are approximately Eddington-limited events. In Section 5 we discuss the implications of our results for the present constraints on, and the future detection of, kilonovae from NS–NS/NS–BH mergers, including the direct constraints that optical transient surveys place on the astrophysical origin of *r*-process elements (Section 5.3.1). We summarize our results and conclude in Section 6.

2 PRELIMINARY CONSIDERATIONS

2.1 Sources of neutron-rich ejecta

There are several potential sources of neutron-rich ejecta from NS–NS/NS–BH mergers. First, neutron-rich material can be ejected due to tidal forces during the merger itself (Lattimer & Schramm 1974; Rosswog et al. 1999; Rosswog 2005). The quantity of this *dynamically ejected* material depends sensitively on the NS–NS/NS–BH binary parameters and the NS equation of state (e.g. Rosswog 2005). Since this material primarily originates from the NS's neutron-rich outer core, it has a typical electron fraction $Y_e \sim 0.03$–0.1 (e.g. Haensel & Zdunik 1990a,b; Rosswog 2005). The electron fraction probably remains low since the ejecta remains cold (and hence thermal weak interactions remain slow) due to adiabatic losses as the material rapidly expands from nuclear densities (e.g. Ruffert et al. 1997; Duez 2009). A typical outflow speed is $v \sim 0.1c$.

Neutron-rich material also originates from outflows from the accretion disc on longer, viscous time-scales. Neutrino-heated winds are driven from the disc for a variety of accretion rates and disc radii during its early evolution (e.g. Metzger et al. 2008b; Surman et al. 2008; Dessart et al. 2009). Although these outflows are generally neutron rich, they can be proton rich in some cases (e.g. Barzilay & Levinson 2008; Metzger, Thompson & Quataert 2008c). An even larger quantity of mass loss occurs at later times once neutrino cooling shuts off, due to powerful outflows driven by viscous heating and the nuclear recombination of free nuclei into α-particles (Metzger et al. 2008b; Lee, Ramirez-Ruiz & López-Cámara 2009; Metzger, Piro & Quataert 2009a). Metzger et al. (2009a) show that $\sim$20–50 per cent of the initial disc mass is ejected with a range of electron fractions $Y_e \sim 0.1$–0.4. The wind's asymptotic speed in this case is also $v \sim 0.1$–$0.2c$, set by the $\sim$8 MeV per nucleon released as heavy elements are formed.

In summary, considering both the tidally and wind-driven ejecta from NS–NS/NS–BH mergers, from $M_{ej} \sim 0$ up to $\sim 0.1\,M_\odot$ in neutron-rich ejecta is expected with $v \sim 0.1c$ and $Y_e \lesssim 0.2$, i.e. sufficiently neutron rich to undergo a robust (low entropy) third-peak *r*-process during its subsequent expansion (e.g. Hoffman, Woosley & Qian 1997). A similar amount of material may be ejected with $Y_e \sim 0.2$–0.4. Although this material is not sufficiently neutron rich to reach the third *r*-process peak, it also produces heavy elements that contribute a comparable radioactive heating rate (Fig. 3).

2.2 Analytic estimates

The majority of the energy released by the *r*-process occurs on a time-scale of $\sim$seconds (e.g. Freiburghaus et al. 1999; Goriely et al. 2005; Metzger et al. 2010). However, most of this initial heating (and any residual heat from the merger itself) is lost to adiabatic expansion because the outflow is highly optically thick at these early times. A significant EM luminosity is only possible once the density decreases sufficiently that photons can escape the ejecta on the expansion time-scale (Arnett 1982). The photon diffusion time through the outflow at radius R is approximately

$$t_d = \frac{B\kappa M_{ej}}{cR}, \tag{1}$$

where κ is the opacity and $B \simeq 0.07$ for a spherical outflow (e.g. Padmanabhan 2000). Setting this equal to the expansion time $t_{exp} = R/v$ gives the characteristic radius for the EM emission to peak

$$R_{peak} \simeq \left(\frac{Bv\kappa M_{ej}}{c}\right)^{1/2} \approx 1.2\times10^{14}\,\mathrm{cm}\left(\frac{v}{0.1c}\right)^{1/2}\left(\frac{M_{ej}}{10^{-2}\,M_\odot}\right)^{1/2}, \tag{2}$$

where we have taken $\kappa = 0.1\,\mathrm{cm^2\,g^{-1}}$ as an estimate of the line opacity of the *r*-process ejecta, assuming it is similar to that of Fe-peak elements (Pinto & Eastman 2000). We discuss the validity of this assumption further in Section 4.1. Assuming free expansion $R = vt$, R_{peak} is reached on a time-scale (Arnett 1982)

$$t_{peak} \approx 0.5\,\mathrm{d}\left(\frac{v}{0.1c}\right)^{-1/2}\left(\frac{M_{ej}}{10^{-2}\,M_\odot}\right)^{1/2}. \tag{3}$$

The above expression is strictly valid only if t_{peak} exceeds the intrinsic radioactive decay lifetime of the ejecta. This condition is generally satisfied for *r*-process ejecta due to their rather short β-decay half-lives. This short time-scale $t_{peak} \sim 1$ d compared to that of a normal SN ($t_{peak} \sim$ weeks) is one of the defining characteristics of kilonovae from NS mergers.

Provided that the radioactive power can be approximated as a decreasing power law in time $\dot{Q} \propto t^{-\alpha}$ with $\alpha < 2$, the brightness of the event depends most sensitively on the amount of radioactive heating that occurs around the time-scale t_{peak}: $Q_{peak} = \int_{t_{peak}} \dot{Q}\,\mathrm{d}t \approx \dot{Q}(t_{peak})t_{peak} = f M_{ej} c^2$, where $f \ll 1$ is a dimensionless number (LP98). Parametrized thus, the peak bolometric luminosity is approximately

$$L_{peak} \simeq \frac{Q_{peak}}{t_d(R_{peak})} \approx 5\times10^{41}\,\mathrm{erg\,s^{-1}}\left(\frac{f}{10^{-6}}\right)\left(\frac{v}{0.1c}\right)^{1/2}\left(\frac{M_{ej}}{10^{-2}\,M_\odot}\right)^{1/2}, \tag{4}$$

and the effective temperature is given by

$$T_{peak} \simeq \left(\frac{L_{peak}}{4\pi R_{peak}^2\sigma}\right)^{1/4} \approx 1.4\times10^4\,\mathrm{K}\left(\frac{f}{10^{-6}}\right)^{1/4}\left(\frac{v}{0.1c}\right)^{-1/8}\left(\frac{M_{ej}}{10^{-2}\,M_\odot}\right)^{-1/8}. \tag{5}$$

Note that $L_{peak} \propto f$, yet the value of f is left as a free parameter in the LP98 model, with values up to $f \sim 10^{-3}$ considered plausible a priori. In Section 3.2 we present explicit calculations of $\dot{Q}$ and show that the effective value of f is $\sim 3\times10^{-6}$. Thus, for $M_{ej} \sim 10^{-2}\,M_\odot$ we expect a transient with peak luminosity $\sim 10^{42}$ erg s^{-1} (bolometric magnitude $M_{bol} \approx -16$) and a photospheric temperature $\sim 10^4$ K, corresponding to a spectral peak at optical/near-UV wavelengths.

3 RADIOACTIVE HEATING

3.1 Network calculations

In this section we present calculations of the radioactive heating of the ejecta. We use a dynamical *r*-process network (Martínez-Pinedo 2008; Petermann et al. 2008) that includes neutron captures, photodissociations, β-decays, α-decays and fission reactions. The latter includes contributions from neutron-induced fission, β delayed fission and spontaneous fission. The neutron capture rates for nuclei with $Z \leq 83$ are obtained from the work of Rauscher & Thielemann (2000) and are based on two different nuclear mass models: the Finite Range Droplet Model (FRDM; Möller et al. 1995) and the Quenched version of the Extended Thomas–Fermi with Strutinsky Integral (ETFSI-Q) model (Pearson, Nayak & Goriely 1996). For nuclei with $Z > 83$ the neutron capture rates and neutron-induced fission rates are obtained from Panov et al. (2010). β-decay rates including emission of up to three neutrons after β-decay are from Möller, Pfeiffer & Kratz (2003). β-delayed fission and spontaneous fission rates are determined as explained by Martínez-Pinedo et al. (2007). Experimental rates for α and β decay have been obtained from the NUDAT data base.[1] Fission yields for all fission processes are determined using the statistical code ABLA (Gaimard & Schmidt 1991; Benlliure et al. 1998). All heating is self-consistently added to the entropy of the fluid following the procedure of Freiburghaus et al. (1999). The change of temperature during the initial expansion is determined using the Timmes equation of state (Timmes & Arnett 1999), which is valid below the density $\rho \sim 3 \times 10^{11}$ g cm^{-3} at which our calculation begins.

As in the *r*-process calculations performed by Freiburghaus et al. (1999), we use a Lagrangian density $\rho(t)$ taken from the NS–NS merger simulations of Rosswog et al. (1999). In addition to $\rho(t)$, the initial temperature T, electron fraction Y_e and seed nuclei properties ($\bar{A}$, $\bar{Z}$) are specified for a given calculation. We assume an initial temperature $T = 6 \times 10^9$ K, although the subsequent *r*-process heating is not particularly sensitive to this choice because any initial thermal energy is rapidly lost to $P\,\mathrm{d}V$ work during the initial expansion before the *r*-process begins (Meyer 1989; Freiburghaus et al. 1999). For our fiducial model we also assume $Y_e = 0.1$, $\bar{Z} \simeq 36$, $\bar{A} \simeq 118$ (e.g. Freiburghaus et al. 1999).

Our results for the total radioactive power $\dot{E}$ with time are shown in Fig. 1. On time-scales of interest the radioactive power can be divided into two contributions: fission and β-decays, which are denoted by dashed and dotted lines, respectively. The large heating rate at very early times is due to the *r*-process, which ends when neutrons are exhausted at $t \sim 1$ s $\sim 10^{-5}$ d. The heating on longer time-scales results from the synthesized isotopes decaying back to stability. On the time-scales of interest for powering EM emission ($t_{\rm peak} \sim$ hours–days; equations3), most of the fission results from the spontaneous fission of nuclei with $A \sim 230$–280. This releases energy in the form of the kinetic energy of the daughter nuclei and fast neutrons, with a modest contribution from γ-rays. The other source of radioactive heating is β-decays of *r*-process product nuclei and fission daughters (see Table 1 for examples corresponding to our fiducial model). In Fig. 1 we also show for comparison the radioactive power resulting from an identical mass of ^{56}Ni and its daughter ^{56}Co. Note that (coincidentally) the radioactive power of the *r*-process ejecta and ^{56}Ni/^{56}Co are comparable on time-scales $\sim$1 d.

[1] http://www.nndc.bnl.gov/nudat2/

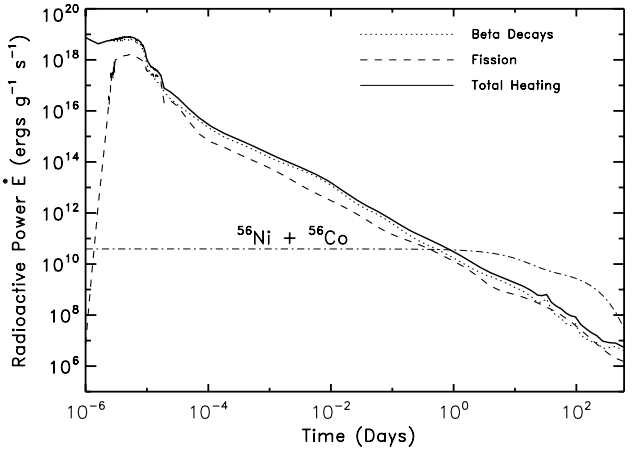

Figure 1. Radioactive heating rate per unit mass $\dot{E}$ in NS merger ejecta due to the decay of *r*-process material, calculated for the $Y_e = 0.1$ ejecta trajectory from Rosswog et al. (1999) and Freiburghaus et al. (1999). The total heating rate is shown with a solid line and is divided into contributions from β-decays (dotted line) and fission (dashed line). For comparison we also show the heating rate per unit mass produced by the decay chain $^{56}\mathrm{Ni} \rightarrow {}^{56}\mathrm{Co} \rightarrow {}^{56}\mathrm{Fe}$ (dot–dashed line). Note that on the $\sim$day time-scales of interest for merger transients ($t \sim t_{\rm peak}$; equation 3) fission and β-decays make similar contributions to the total *r*-process heating, and that the *r*-process and ^{56}Ni heating rates are similar.

Table 1. Properties of the dominant β-decay nuclei at $t \sim 1$ d.

Isotope	$t_{1/2}$ (h)	Q[a] (MeV)	$\epsilon_{\rm e}^b$	ϵ_ν^c	ϵ_γ^d	$E_\gamma^{{\rm avg}\,e}$ (MeV)
^{135}I	6.57	2.65	0.18	0.18	0.64	1.17
^{129}Sb	4.4	2.38	0.22	0.22	0.55	0.86
^{128}Sb	9.0	4.39	0.14	0.14	0.73	0.66
^{129}Te	1.16	1.47	0.48	0.48	0.04	0.22
^{132}I	2.30	3.58	0.19	0.19	0.62	0.77
^{135}Xe	9.14	1.15	0.38	0.40	0.22	0.26
^{127}Sn	2.1	3.2	0.24	0.23	0.53	0.92
^{134}I	0.88	4.2	0.20	0.19	0.61	0.86
^{56}Ni[f]	146	2.14	0.10	0.10	0.80	0.53

[a] Total energy released in the decay.
[b,c,d] Fraction of the decay energy released in electrons, neutrinos and γ-rays.
[e] Average photon energy produced in the decay.
[f] Note: ^{56}Ni is not produced by the *r*-process and is only shown for comparison [although a small abundance of ^{56}Ni may be produced in accretion disc outflows from NS–NS/NS–BH mergers (Metzger et al. 2008b)].

In Fig. 2 we show the final abundance distribution from our fiducial model, which shows the expected strong second and third *r*-process peaks at $A \sim 130$ and $\sim$195, respectively. For comparison, we show the measured Solar system *r*-process abundances with points. The computed abundances are rather different to the one obtained by Freiburghaus et al. (1999) due to an improved treatment of fission yields and freeze-out effects.

Although we assume $Y_e = 0.1$ in our fiducial model, the ejecta from NS mergers will possess a range of electron fractions (see Section 2.1). To explore the sensitivity of our results to the ejecta composition we have run identical calculations of the radioactive heating, but varying the electron fraction in the range $Y_e = 0.05$–0.35. Although in reality portions of the ejecta with different compositions will undergo different expansion histories, in order to make a direct comparison we use the same density trajectory $\rho(t)$ as was described earlier for the $Y_e = 0.1$ case. Fig. 3 shows the heating rate

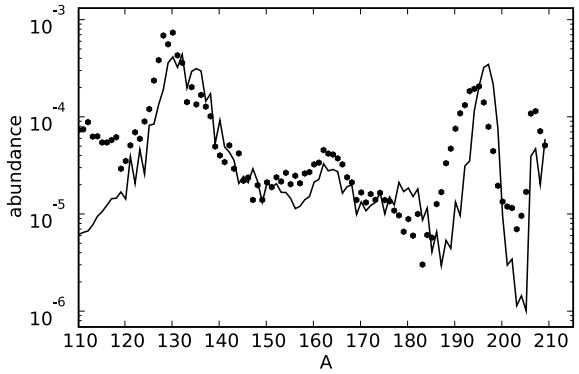

Figure 2. Final abundance distribution from the fiducial model with $Y_e = 0.1$ (Fig. 1), shown as the mass fraction versus mass number A. Measured Solar system r-process abundances are shown for comparison with black dots. They are arbitrarily normalized to the computed abundances for $A = 195$.

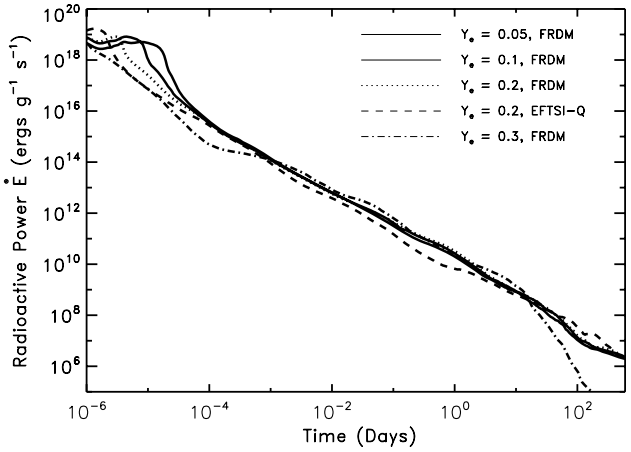

Figure 3. Total radioactive heating rate per unit mass $\dot{E}$, calculated for several values of the electron fraction Y_e of the ejecta and for different nuclear mass models (see text). Calculations employing the FRDM mass model (Möller et al. 1995) are shown for $Y_e = 0.05$ (triple dot–dashed line), $Y_e = 0.1$ (solid line), $Y_e = 0.2$ (dotted line) and $Y_e = 0.3$ (dot–dashed line). A calculation employing the EFTSI-Q (Pearson et al. 1996) mass model is shown for $Y_e = 0.2$ (dashed line). Note that on time-scales of hours–days, the radioactive heating rates in all models agree to within a factor of $\sim$4.

for ejecta with $Y_e = 0.05$, 0.2 and 0.3 in comparison to the fiducial model with $Y_e = 0.1$. Although the heating rate for different values of Y_e differs substantially at early times ($\lesssim 10^{-4}$ d), $\dot{E}$ agrees between the models to better than a factor of $\sim$2 at the later times that are the most important for transient EM emission.

Our results for $\dot{E}$ could in principle also be sensitive to the assumed properties of the nuclei in the r-process path (e.g. masses and neutron-capture cross-sections), which are uncertain and must be obtained via theoretical modelling. In our fiducial model (Fig. 1) we employ the FRDM model (Möller et al. 1995) for nuclear masses. In order to explore the sensitivity of our results to the assumed nuclear physics, we also performed an otherwise identical calculation using the ETFSI-Q mass model (Pearson et al. 1996), as shown in Fig. 3 for $Y_e = 0.2$. Although the two models again differ in their early-time predictions for $\dot{E}$, on time-scales $\gtrsim$1 h they converge to a heating rate within a factor of $\lesssim$4.

Finally, although the Lagrangian density trajectory $\rho(t)$ that we employ in our fiducial model formally corresponds to dynamically ejected rather than wind-driven ejecta, both are likely present in NS–NS/NS–BH mergers (see Section 2.1). Thus, we have also performed an otherwise identical calculation, but instead using a trajectory $\rho(t)$ appropriate for (higher entropy) disc winds, similar to those studied in e.g. Arcones, Janka & Scheck (2007) (cf. Metzger et al. 2008b; Surman et al. 2008). Although we do not show our results explicitly in this case, we find that the heating rate $\dot{E}$ decreases in a similar manner to the dynamically ejected material on time-scales $\sim$1 d. However, the overall normalization of $\dot{E}$ is smaller by a factor of $\sim$10 because in high-entropy winds the mass fraction of heavy nuclei is reduced at the expense of a higher α-particle fraction, which do not contribute to the heating (Hoffman et al. 1997). Although some of the wind-driven material in NS mergers may have high entropy (Metzger et al. 2008c; Surman et al. 2008), most of the total mass ejected likely has low-modest entropy ($S \sim 3$–$10\,k_b$ baryon^{-1}; Metzger et al. 2009a). When correcting our results for the higher mass fraction of heavy nuclei in a lower entropy wind, we find that the heating rate $\dot{E}$ on time-scales $\sim$1 d in the wind ejecta agrees within a factor of $\sim$2 to that of the dynamically ejected material.

To summarize, the heating rate for our fiducial model in Fig. 1 (which we employ throughout the remainder of the paper) appears to be relatively insensitive to the precise trajectory and composition of the ejecta, and to the uncertainties in the nuclear properties of the unstable nuclei near the r-process path.

In order to understand why we find such a robust heating rate on time-scales $\sim$1 d, it is first instructive to compare r-process ejecta with that produced in Type Ia SNe. In Type Ia SNe, the ejected material is processed through nuclear statistical equilibrium with $Y_e \approx 0.5$. This favours the production of $N = Z$ nuclei and, in particular, ^{56}Ni. The ^{56}Ni nucleus ($N = Z = 28$) is produced in high abundance both because 28 is a magic nucleon number and because even–even ($N = Z$) nuclei have an additional binding energy, commonly known as the 'Wigner energy'. At the high temperatures at which ^{56}Ni is produced, atoms are fully ionized and, consequentially, ^{56}Ni cannot decay by atomic electron capture. In this case the half-life has been computed to be $t_{1/2} \approx 4 \times 10^4$ yr by Fisker, Martínez-Pinedo & Langanke (1999). Once the temperature decreases sufficiently that the inner K-shell orbit electrons recombine, the decay proceeds at the laboratory measured rate $t_{1/2} \simeq 6.075(10)$ d (da Cruz et al. 1992).

The situation is different for neutron-rich r-process ejecta. First, r-process nuclei decay by β^- and hence the half-life is unaffected by the ionization state of the matter. Secondly, the r-process results in a rather broad distribution of nuclei with mass number spanning the range $A \sim 110$–210. Because the nuclei produced in NS mergers likely follow a distribution similar to their solar system abundances (see Fig. 2), maxima will occur at the second ($A \sim 130$) and third ($A \sim 195$) r-process peaks. The *overall* r-process abundances peak in our calculations (as in the Solar system) near the second peak, which is why second-peak nuclei dominate the β-decay heating rate (see Table 1).

We argue below, however, that the energy generation rate $\dot{E}$ is approximately *independent of the precise distribution of heavy nuclei*, provided that the heating is not dominated by a few decay chains and that statistical arguments can be applied. This conclusion is supported by our results in Fig. 3, which show that $\dot{E}$ is relatively insensitive to the composition of the ejecta, despite the fact that different electron fractions can result in rather different abundance distributions. Perhaps most striking, the heating rate is similar whether the second r-process peak is produced via the fission of nuclei near the magic neutron numbers $N = 184$ ($A \sim 280$),

as occurs for highly neutron-rich ejecta ($Y_e \lesssim 0.2$), or whether it is produced directly with little or no fission cycling, as occurs for $Y_e \gtrsim 0.3$.

Assuming a broad distribution of exponentially decaying nuclei with mass number A the evolution of the energy generation rate $\dot{E}$ can be understood by the following arguments. For an isotopic chain of odd-A nuclei the Q values are essentially proportional to the neutron excess $\eta \equiv N - Z$ and the β-decay rate $\lambda \propto \eta^5$ due to the three-body nature of the final state. The situation is slightly more complicated for even-A chains due to the presence of pairing that increases the binding energy of even–even nuclei and modifies the global proportionality of the Q value and neutron excess. However, the selection rules of β-decay favour a maximum change in angular momentum between initial and final states of one unit; as a result, the decay of odd–odd nuclei, that typically have angular momentum $J > 1$, proceeds via excited states in the daughter even–even nucleus. Consequently, the global dependence $\lambda \propto \eta^5$ is recovered. Assuming that the number of nuclei per neutron excess interval is constant the number of nuclei per decay rate interval, λ, and lifetime interval, $\tau = 1/\lambda$, are given by

$$\mathrm{d}N = N_0 \lambda^{-4/5}\,\mathrm{d}\lambda, \quad \mathrm{d}N = N_0 \tau^{-6/5}\,\mathrm{d}\tau, \tag{6}$$

where N_0 is a normalization constant. Further assuming that the energy generation at a time t is dominated by nuclei with $\tau = t$ that release energy $Q \propto \tau^{-1/5}$, the energy generation rate then becomes

$$\dot{E} \propto t^{-7/5} = t^{-1.4}. \tag{7}$$

The same result can be obtained assuming that we have a distribution of nuclei that follows equation (6), each releasing an energy $Q \propto \lambda^{1/5}$ with a rate λ. In this case the energy generation rate is

$$\dot{E} \propto \int_0^\infty \lambda \lambda^{1/5}\,\mathrm{e}^{-\lambda t} N_0 \lambda^{-4/5}\,\mathrm{d}\lambda = N_0 \Gamma(7/5) t^{-7/5}, \tag{8}$$

where Γ is the Gamma function.

The above discussion neglects the fact that with increasing neutron excess the β-decay populates an increasing number of states in the daughter nucleus. Consequently, we expect an exponent slightly larger than 5 for the dependence of decay rates with neutron excess. This will result in a power-law decay with an exponent smaller than the value of 1.4 deduced above. Overall, this analytic derivation is in reasonable agreement with the numerical results in Fig. 1, which correspond to $\dot{E} \propto t^{-\alpha}$ with $\alpha \sim 1.1$–1.3 on time-scales of hours–days. Incidentally, we note that this functional form is remarkably similar to the heating rate $\dot{E} \propto t^{-1.2}$ found for the decay of nuclear waste from terrestrial reactors (Cottingham & Greenwood 2001, p. 126).

3.2 Thermalizing processes

Of the total power released by nuclear reactions $\dot{E}$ (Fig. 1), only a fraction $\epsilon_{\rm therm}$ will thermalize with the plasma and hence be useful for powering EM emission. In this section we estimate $\epsilon_{\rm therm}$. Since the light-curve peaks on approximately the time-scale $t_{\rm peak}$ (equation 3), we shall normalize our considerations to this time.

3.2.1 β-decay heating

First, consider the energy released by β-decays, which dominate $\dot{E}$ at late times (Fig. 1). The total energy released in the decay Q is divided between the outgoing neutrino and electron, and the γ-rays produced as the daughter nucleus cascades to the ground state from excited nuclear levels. In Table 1 we list the properties of a sample of nuclei which contribute appreciably to $\dot{E}$ at $t \sim t_{\rm peak} \sim 1$ d, as determined from our network calculations in Section 3.1. The properties listed include the decay half-life $t_{1/2}$, the relative fraction of Q carried away by the electron, neutrino and γ-rays (ϵ_e, ϵ_ν and ϵ_γ, respectively) and the mean γ-ray energy $E_\gamma^{\rm avg}$. Most of this information was obtained or calculated using data from the Lawrence Berkeley National Laboratory's Isotopes Project.[2]

Because the energy imparted to the outgoing electron $E_e = \epsilon_e\, Q$ is generally greater than or similar to the electron rest mass (0.511 MeV), the electron is mildly relativistic and, as a result, carries a similar fraction of the outgoing energy as the neutrino (i.e. $\epsilon_e \approx \epsilon_\nu$). Although the neutrino readily escapes the ejecta and does not contribute to the heating, the electron is charged and interacts electromagnetically with the ambient electrons and nuclei. The dominant thermalizing process is electron–electron coulomb scattering.

For electron–electron scattering in the fast test particle limit ($E_e \gg kT$, where $T \sim 10^4$ K is the temperature of the background plasma), the energy exchange (or 'thermalization') time-scale is given by

$$t_{\rm therm}^{e-e} \approx 4.6 \times 10^{13}\ \mathrm{s} \left(\frac{E_e}{0.5\,\mathrm{MeV}}\right)^{3/2} \ln\Lambda^{-1} n_e^{-1}, \tag{9}$$

where $\ln\Lambda$ is the Coulomb logarithm (e.g. *NRL Plasma Formulary*; Huba 2007). Assuming a spherical, homogeneous outflow, the electron density n_e at time t is approximately given by

$$n_e = \frac{M_{\rm ej}}{(4\pi/3) R^3 \mu_e} \approx 10^{12}\,\mathrm{cm}^{-3} \left(\frac{M_{\rm ej}}{10^{-2}\,\mathrm{M}_\odot}\right)^{-1/2} \left(\frac{v}{0.1c}\right)^{-3/2} \left(\frac{t}{t_{\rm peak}}\right)^{-3}, \tag{10}$$

where $\mu_e \approx A m_n / Z$ is the mean mass per electron, m_n is the mass of a nucleon, and we have assumed an average charge $Z \sim 60$ and mass $A \sim 130$ for the r-process nuclei. Although the r-process nuclei are only partially ionized on time-scales $t \sim t_{\rm peak}$, n_e includes both free and bound electrons because, for purposes of high-energy scattering, they have identical cross-sections (the impact parameter for $E_e \sim$ MeV is much smaller than the atomic scale).

Thus, the ratio of the thermalization time due to electron–electron collisions $t_{\rm therm}^{e-e}$ to the time-scale at which the emission peaks is given by

$$t_{\rm therm}^{e-e}/t_{\rm peak} \approx 10^{-4} \left(\frac{E_e}{0.5\,\mathrm{MeV}}\right)^{3/2} \left(\frac{\ln\Lambda}{10}\right)^{-1} \left(\frac{v}{0.1c}\right)^{2} \left(\frac{t}{t_{\rm peak}}\right)^{3}. \tag{11}$$

Equation (11) shows that for a typical value $E_e \sim 0.5$ MeV, $t_{\rm therm}^{e-e} > t_{\rm peak}$ for $t \lesssim 10 t_{\rm peak}$, implying that the β-decay electrons will efficiently thermalize on the time-scales of interest.

Table 1 shows that typically $\sim$1/2 of the β-decay energy is also released in the form of $\sim$MeV γ-rays. Although a portion of the γ-rays will thermalize via Compton scattering and photoelectric absorption (e.g. Colgate, Petschek & Kriese 1980; Swartz, Sutherland & Harkness 1995), a significant fraction will also escape, especially as the ejecta expands and the optical depth decreases. In the case of ^{56}Ni and ^{56}Co, for example, Swartz et al. (1995) find an effective absorptive opacity which is about $\sim$15 per cent of the fully ionized Thomson opacity (i.e. $\kappa_\gamma \approx 0.03\,\mathrm{cm}^2\,\mathrm{g}^{-1}$) using Monte Carlo

[2] http://ie.lbl.gov/education/

radiative transfer calculations. Since $t_{\rm peak}$ is attained when the optical depth is $\tau_{\rm peak} \sim c/v \sim 10$, the thermalization 'optical depth' is $\lesssim 1$ for times greater than $\approx (\kappa/\kappa_\gamma)(v/c)t_{\rm peak} \sim t_{\rm peak}$ (see equations 1 and 3). As Table 1 illustrates, the mean γ-ray energy $E_\gamma^{\rm avg}$ from ^{56}Ni decay is within a factor of $\sim$2 of those produced by the other β-decays, so we expect similar γ-ray thermalization properties in Type Ia SNe and in NS merger ejecta. We conclude that photons will partially thermalize for $t \lesssim t_{\rm peak}$, but they will contribute little heating at later times ($t \gg t_{\rm peak}$).

From Table 1 we infer average values of $\epsilon_{\rm e} \approx \epsilon_\nu \approx 0.25$ and $\epsilon_\gamma \approx 0.5$ (Table 1). Combining our results, we conclude that the effective β-decay thermalization fraction will vary from $\epsilon_{\rm therm} \approx \epsilon_{\rm e} + \epsilon_\gamma \approx 0.75$ to $\epsilon_{\rm therm} \approx \epsilon_{\rm e} \approx 0.25$ as the ejecta expands from $R \ll R_{\rm peak}$ to $R \gtrsim R_{\rm peak}$.

3.2.2 *Fission heating*

In the case of fission most of the radioactive energy is released as kinetic energy of the fission product nuclei, with a typical daughter energy of $E_A \sim 100\,{\rm MeV}$. In this case the dominant thermalizing process is Coulomb scattering off ambient nuclei of similar mass A and charge Z. In the case of ion–ion collisions the thermlization time-scale is (Huba 2007)

$$t_{\rm therm}^{A-A} \approx 5 \times 10^{12}\,{\rm s}\,\ln\Lambda^{-1} n_A^{-1} \left(\frac{E_A}{100\,{\rm MeV}}\right)^{3/2} \left(\frac{A}{130}\right)^{1/2} \left(\frac{Z}{60}\right)^{-4}, \quad (12)$$

where $n_A \approx \rho/Am_{\rm n}$ is the number density of ambient nuclei. Thus, using equations (3) and (10) the ratio of the thermalization time-scale to the time-scale at which the emission peaks is given by

$$t_{\rm therm}^{A-A}/t_{\rm peak} \approx 6 \times 10^{-3} \left(\frac{E_A}{100\,{\rm MeV}}\right)^{3/2} \left(\frac{A}{130}\right)^{3/2} \times \left(\frac{Z}{60}\right)^{-4} \left(\frac{\ln\Lambda}{10}\right)^{-1} \left(\frac{v}{0.1c}\right)^2 \left(\frac{t}{t_{\rm peak}}\right)^3. \quad (13)$$

Since $t_{\rm therm}^{A-A} \ll t_{\rm peak}$ we conclude that the fission daughters will also thermalize on time-scales $\sim t_{\rm peak}$, implying that $\epsilon_{\rm therm} \approx 1$ for fission. Therefore, even though fission contributes less to $\dot{E}$ than β-decays at $t \sim t_{\rm peak} \sim 1$ d, its higher thermalized fraction suggests that it may dominate the heating.

3.2.3 *Neutron heating*

Neutrons, emitted either spontaneously following fission or induced by β-decays, also carry a modest portion of the released energy. Although the contribution of neutrons to $\dot{E}$ is generally much less than that of β-decays or the kinetic energy of fission daughters, we consider their thermalization as well for completeness.

At high densities (e.g. in terrestrial reactors) fission-product neutrons can be captured by heavy nuclei to induce further reactions. For the much lower densities of present interest, however, the neutron capture time-scale (with a typical cross-section $\sim$ millibarns) is much longer than the free neutron β-decay time-scale $\sim$15 min. As a result, fast neutrons created by fission rapidly decay into fast protons (with a typical energy $E_{\rm p} \sim 1$ MeV) before capturing. In order to thermalize, the protons must exchange energy with the much heavier ambient charged particles (the proton density is too low for p–p scattering to be efficient). We find that the proton's thermalization time is larger by a factor $\sim Z^2 A^{1/2}(E_p/E_A)^{3/2} \sim 10^2$ than that of the fission daughter nuclei (equation 13). This suggests that the proton will have $t_{\rm therm} \sim t_{\rm peak}$ and hence may not thermalize.

Our estimates above neglect, however, the possible effects of magnetic fields, which can trap charged particles and enhance their thermalization if the field is directed perpendicular to the outflow velocity (e.g. Colgate et al. 1980). For instance, if the NS involved in the merger has a (modest) surface field strength of $B \approx 10^9$ G, this translates into a field strength of $B \sim 3 \times 10^{-8}$ G at $R \sim R_{\rm peak}$ by flux freezing. The Larmor radius for a 1-MeV proton at $R_{\rm peak}$ is $r_{\rm L} \sim 10^{12}$ cm, which is $\ll R_{\rm peak} \sim 10^{14}$ cm. This suggests that the proton's residence time (and hence thermalization) may be significantly enhanced due to the magnetic field. As a result, we conclude that the energy released in neutrons will also likely thermalize.

3.2.4 *Net heating efficiency and the effective value of f*

Considering both β-decays (with $\epsilon_{\rm therm} \approx 0.25$–$0.75$) and fission ($\epsilon_{\rm therm} \approx 1$), we conclude that the net heating fraction of merger ejecta is between $\epsilon_{\rm therm} \approx 0.25$ and $\approx$1, depending on time and the relative contributions of β-decays and fission to $\dot{E}$.

From Fig. 1 we find that $\dot{E}$ decreases approximately as a power law $\dot{E} \propto t^{-\alpha}$, with a value $\alpha \sim 1.1$–1.4 on time-scales of hours–days, relatively close to the heating functional form adopted by LP98: $\dot{Q} \propto fc^2/t$ (see equation 4 and surrounding discussion). In Section 3.1 we presented a simple derivation of this result that explains why $\alpha \lesssim 1.4$ (see equations 7 and 8). For an average thermalization efficiency of $\epsilon_{\rm therm} \sim 0.75$, our results imply that the *effective value* of f is $\approx 3 \times 10^{-6}$ at $t \sim 1$ d. This is somewhat lower than the range of values considered by LP98 and much lower than has been estimated elsewhere in the literature. For instance, Rosswog (2005) estimates a NS merger transient peak luminosity $L_{\rm peak} \sim 10^{44}\,{\rm erg\,s^{-1}}$, corresponding to an effective value of $f \sim 10^{-3}$ for $M_{\rm ej} \sim 10^{-2}\,{\rm M}_\odot$ (equation 4). He derives this under the assumption that an appreciable fraction of the total energy released in forming heavy r-process nuclei ($B/A \sim 8\,{\rm MeV\,nucleon^{-1}}$) is released over a time-scale $t_{\rm peak} \sim 1$ d. This is incorrect because *most* of the binding energy is released by the formation of seed nuclei in the initial expansion (on time-scales $\sim$ milliseconds) and by the subsequent r-process (on time-scales $\lesssim 1$ s; see Fig. 1). Since this heating all occurs at radii $R \lesssim (v \times 1\,{\rm s}) \sim (v/0.3c)10^{10}$ cm, this early-time heating suffers a factor of $\gtrsim 10^4$ loss in thermal energy due to $P\,{\rm d}\,V$ work before the outflow expands to the radius $R_{\rm peak} \sim 10^{14}$ cm (equation 2) at which photons can finally escape. Instead, the luminosity at $t \sim t_{\rm peak}$ is primarily powered by *residual* energy released as r-process products fission and decay back to stability. This occurs on much longer time-scales and involves a significantly smaller energy release (typically closer to $\sim 10^{-3}\,{\rm MeV\,nucleon^{-1}}$ on time-scales $\sim$1 d).

4 LIGHT CURVES

4.1 Radiative transfer calculation

We calculate the light curves of compact object merger ejecta using the time-dependent radiative transfer code SEDONA (Kasen, Thomas & Nugent 2006). Our set-up is similar to that described in Darbha et al. (2010) for the case of ^{56}Ni decay-powered transients produced by the accretion-induced collapse of white dwarfs. However, in the present case we have modified the code to include the radioactive heating $\dot{Q} = \epsilon_{\rm therm}\dot{E}$ for NS mergers as calculated in Section 3. Although SEDONA can track γ-ray thermalization, we do not use this

option given the large number of decaying nuclei and their complex γ-ray spectra; rather, we incorporate the escape fraction into an average thermalization efficiency $\epsilon_{\rm therm}$ that we hold constant in time. We calculate models assuming both $\epsilon_{\rm therm} = 0.5$ and 1 in order to bracket the uncertainty in the precise fraction of γ-rays that thermalize (see Section 3.2.4).

Although the ejecta from NS–NS/NS–BH mergers is likely to be highly asymmetric (e.g. the 'banana-like' geometry of tidal tails; Rosswog 2005), we assume a one-dimensional (spherically symmetric) geometry for simplicity. We shall address the effects of the full multidimensional kinematics of the outflow in future work. Since SEDONA uses a velocity–time grid, a required input to the calculation is the velocity profile $\rho(v)$ of the (assumed homologous) expansion. We take the density profile to decrease as $\rho \propto v^{-3}$ between $v \approx 0.05$–$0.2c$, as motivated by the typical velocity $v \sim 0.1c$ of the dynamically ejected and wind-driven neutron-rich ejecta from NS–NS/NS–BH mergers (Section 2.1). We assume that $\rho(v)$ decreases exponentially with v outside this range and have verified that our results are not sensitive to precisely how we taper the edges of the velocity distribution. We find that our results are also similar if we instead assume $\rho \propto v^{-2}$ or $\rho \propto v^{-4}$, implying that the exact density profile is not crucial for the overall light-curve shape.

Another input to our calculation is the composition, the ionization energies of each element and the bound–bound and bound–free opacities of each element. Unfortunately, the spectral line information for these very high-Z elements is very limited. Most of the data available is experimental (e.g. Lawler et al. 2006, 2007, 2009; Biémont et al. 2007), since many body quantum mechanical calculations of these elements' spectra represent a formidable task, even with modern computing. Much of the experimental work has focused on aiding studies of r-process abundances in ultra metal-poor halo stars, which generally make use of resonant absorption lines at optical wavelengths (e.g. Cayrel 1996; Sneden et al. 2003). However, the total *opacity* of most relevance to merger transients results from densely packed UV lines, for which there is currently insufficient information in either the Kurucz line list (Kurucz & Bell 1995) or the more recent experimental studies. Nevertheless, the spectra of at least some high-Z r-process elements are almost certainly as complex as Fe peak elements, if not more (Wahlgren, private communication); this is important because the Fe peak elements cause UV 'line blanketing' in normal SN spectra. We expect that the same effect is likely to be produced by third r-process peak elements since they are largely transition metals.

Given this lack of spectral information, we attempt to crudely account for the effects of the unknown r-process element lines on the opacity by using the bound–bound lines of Fe, but modified to include the correct ionization energies of the r-process elements. Specifically, our calculations use the ionization energies of Pb as a representative r-process element. These uncertainties in the bound–bound transitions obviously limit our ability to make detailed spectroscopic predictions, but it does allow us to qualitatively address the effects of line blanketing on the transients' colour evolution. In addition, the overall light-curve shape, the peak luminosity and the characteristic time-scale of the event ($\sim$ day) are robust in spite of these uncertainties.

4.2 Results

Fig. 4 shows our results for the bolometric light curve for a fiducial model with $Y_{\rm e} = 0.1$, ejecta mass $M_{\rm ej} = 10^{-2}\,{\rm M}_{\odot}$ and outflow speed $v = 0.1c$. We show two calculations performed using different values for the assumed thermalization efficiency, $\epsilon_{\rm therm} = 0.5$ and 1, which roughly bracket our uncertainty in the γ-ray escape fraction (Section 3.2). Also shown for comparison in Fig. 4 is the toy model of LP98 (cf. Kulkarni 2005; Section 2.2), calculated assuming an electron scattering opacity and an 'f' value $= 3 \times 10^{-6}$, as calibrated to match the radioactive heating rate in Section 3.2.4. Fig. 4 shows that the light curves predicted using the toy model and our more detailed calculation are relatively similar near the time of peak emission ($t_{\rm peak} \sim 1$ d), but their differences become more pronounced at earlier and later times. The 'bumps' in the light curve at $t \sim$ few days in our calculation are due to recombination of the outer shell electrons in our representative high-Z element Pb (and the resulting opacity change) as the expanding photosphere cools.

In the top panel of Fig. 5 we decompose the light curve into luminosities νL_ν in several standard optical bands (i.e. 'colours'). The bottom panel of Fig. 5 shows the analogous colour evolution predicted with the LP98 model, which assumes a perfect (single temperature) blackbody spectrum. Both calculations predict that the

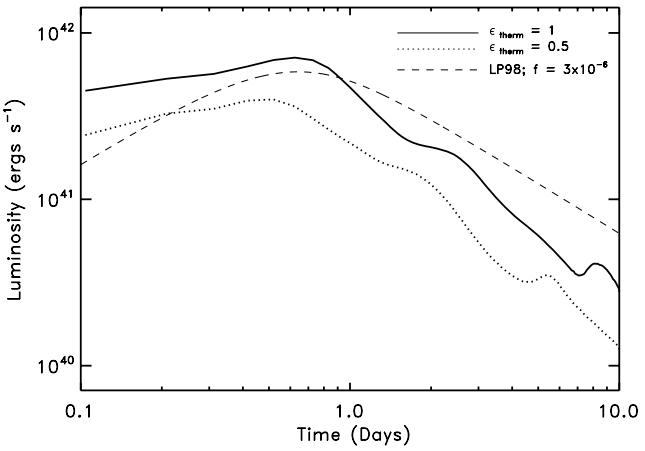

Figure 4. Bolometric light curve of the radioactively powered transients from NS–NS/NS–BH mergers, calculated assuming a total ejecta mass $M_{\rm tot} = 10^{-2}\,{\rm M}_{\odot}$ with electron fraction $Y_{\rm e} = 0.1$ and mean outflow speed $v \simeq 0.1c$, and for two values of the thermalization efficiency (Section 3.2), $\epsilon_{\rm therm} = 1$ (solid line) and $\epsilon_{\rm therm} = 0.5$ (dotted line). Also shown for comparison (dashed line) is a one-zone calculation based on the LP98 model (as implemented in Kulkarni 2005; Metzger et al. 2008b) assuming $f = 3 \times 10^{-6}$ (see Section 3.2.4) and the same values for $M_{\rm tot}$ and v.

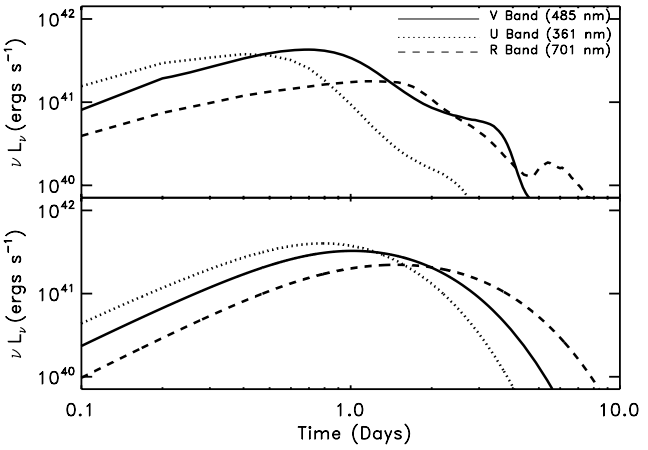

Figure 5. Top panel: νL_ν colour light curves from the $\epsilon_{\rm therm} = 1$ calculation in Fig. 4. V-, U- and R-band light curves are shown with solid, dotted and dashed lines, respectively. Bottom panel: analogous colour evolution predicted by the LP98 blackbody model.

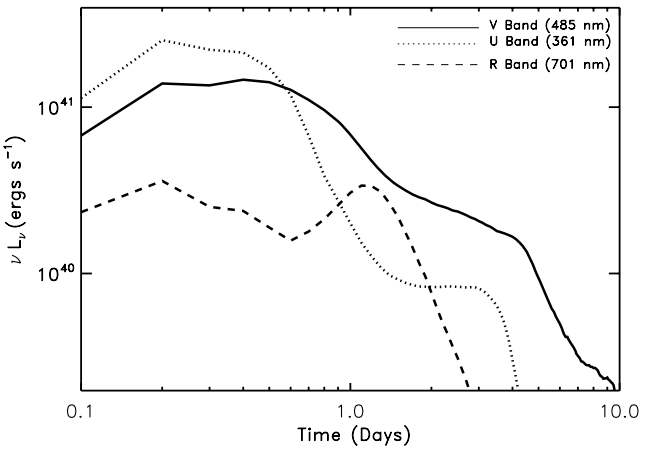

Figure 6. Same as the top panel in Fig. 5, but calculated for $M_{\rm ej} = 10^{-3}\,{\rm M}_\odot$.

light-curve peaks earlier in time at shorter wavelengths because the photospheric temperature decreases with time as the ejecta expands. However, the LP98 model predicts an overall νL_ν peak in the UV, while our calculation predicts an earlier peak at longer wavelengths (i.e. in V band) and a clear suppression in UV emission at times $t \gtrsim 1$ d. This behaviour results from strong UV absorption due to dense bound–bound transitions ('line blanketing'), which produces a much redder spectrum than would be predicted by assuming a grey opacity. Indeed, rapid reddening following the peak emission epoch is likely a defining characteristic of kilonovae.

We have also explored the sensitivity of our results to the mass of the ejecta by performing an otherwise identical calculation, but with a lower ejecta mass $M_{\rm ej} = 10^{-3}\,{\rm M}_\odot$. Our results for the colour evolution are shown in Fig. 6. Although the qualitative features of the light-curve evolution are similar to the $M_{\rm ej} = 10^{-2}\,{\rm M}_\odot$ case, the V-band light-curve peaks somewhat earlier and at a lower luminosity, as expected from the analytic scaling relationships $t_{\rm peak} \propto M_{\rm ej}^{1/2}$ (equation 3) and $L_{\rm peak} \propto M_{\rm ej}^{1/2}$ (equation 4). The higher photosphere temperature at the epoch of peak emission for lower $M_{\rm ej}$ ($T_{\rm peak} \propto M_{\rm ej}^{-1/8}$; equation 5) also results in somewhat bluer peak emission.

5 DETECTION PROSPECTS

Because the radioactively powered emission from NS–NS/NS–BH mergers is relatively isotropic, it can in principle be detected in at least three independent ways: (1) coincident with a source of detected GWs; (2) coincident with a short-duration GRB and (3) via blind transient surveys (e.g. PTF and LSST). In this section, we discuss each possibility in turn.

5.1 Gravitational wave-triggered follow-up

Advanced LIGO is expected to be sensitive to NS–NS and NS–BH mergers out to a distance ∼300 and ∼650 Mpc, respectively (Cutler & Thorne 2002). For an ejecta mass of $M_{\rm ej} = 10^{-2}\,{\rm M}_\odot$ we predict a peak V-band luminosity of $\approx 3 \times 10^{41}\,{\rm erg\,s^{-1}}$ (Fig. 4), corresponding to an absolute magnitude $M_V \sim -15$. Thus, the entire Advanced LIGO volume could be probed by searching down to magnitude $V \sim 22$–24. Although this represents a realistic depth for a moderately large telescope, the positional uncertainty of LIGO/Virgo detections is expected to range from many arcminutes to degrees (e.g. Sylvestre 2003). As a result, both sensitivity and a large field of view (i.e. a high 'étendue') are requirements for any follow-up instrument. Since these figures of merit are already optimized for transient survey telescopes, projects such as PTF and (eventually) LSST and SASIR may be optimal for GW follow-up (in addition to their role in blind transient searches; Section 5.3).

Given the short-lived duration ∼1 d of the expected transient signal, rapid GW data reduction (e.g. Márka, Mours & Williams 2002) and dissemination of candidate detections to the astronomical community will be crucial for detection and follow-up (as has been adopted by the neutrino community; e.g. Kowalski & Mohr 2007; Abbasi et al. 2009; Stamatikos et al. 2009). Indeed, given the unique optical signature of NS–NS/NS–BH merger transients (Section 4), moderately deep optical/NIR follow-up of even low-significance potential GW sources could improve the effective sensitivity of Advanced LIGO/Virgo with only a relatively moderate investment of resources (see Kowalski & Mohr 2007 for an example applied to high-energy neutrino point sources). This could prove to be particularly important if the merger rates are at the low end of current estimates. Recently, efforts have begun to set up a rapid GW data analysis pipeline to produce location-probability sky maps within ∼5–10 min following a GW detection with LIGO/Virgo (Kanner et al. 2008). In fact, a pilot program for the prompt follow-up of GW triggers with wide-field optical telescopes such as QUEST and TAROT is already underway (Shawhan, private communication).

5.2 Short-duration GRB follow-up

Given the possible association between short-duration GRBs and NS–NS/NS–BH mergers, another method to search for kilonovae is with deep optical/IR observations on ∼1 d time-scale following the burst. Recently, Kocevski et al. (2010) presented upper limits on the presence of a putative LP98 kilonova using follow-up observations of GRB 070724A and GRB 050509b (Hjorth et al. 2005). Our results in Section 4.2 show that the LP98 model (properly calibrated) does a reasonably good job of reproducing the qualitative features of the optical/NIR light curves around the time of peak emission. Thus, by assuming $v \approx 0.1c$ and $f \approx 3 \times 10^{-6}$ (Section 3.2.4) we conclude from their figs 8 and 9 that $M_{\rm ej}$ must be $\lesssim 0.1$ and $\lesssim 10^{-3}\,{\rm M}_\odot$ for GRBs 070724A and 050509b, respectively. Although the former (070724A) is not particularly constraining on merger models because such a large ejecta mass is unlikely, the latter non-detection (050509b) suggests that the disc that formed in this event was rather small ($\lesssim 10^{-2}\,{\rm M}_\odot$; see the discussion in Section 2.1). A low disc mass is, however, still consistent with a merger interpretation for this event because the isotropic luminosity of the GRB was quite low ($E_{\gamma,{\rm iso}} \sim 2.4 \times 10^{48}$ erg; Kann et al. 2008): even ignoring geometric beaming corrections, only an accreted mass $\sim 10^{-5}\,{\rm M}_\odot$ is necessary to produce a relativistic jet with energy $E_{\gamma,{\rm iso}}$ assuming that the efficiency for converting rest-mass energy to γ-ray power is ∼10 per cent (e.g. McKinney 2005).

Berger (2009) present additional early optical/NIR follow-up observations of GRB 070724a, including the discovery of transient emission peaking $t \sim 3$ h following the burst. Because of the transient's very red spectrum (which is highly unusual for a standard GRB afterglow) they suggest a possible NS merger transient interpretation. They conclude, however, that this possibility is unlikely: the brightness and rapid rise time of the transient require values of $f \sim 5 \times 10^{-3}$ and $M_{\rm ej} \sim 10^{-4}\,{\rm M}_\odot$ which, within the standard LP98 model, predicts a photospheric temperature peaked in the UV (equation 3) and thus inconsistent with the transient's red colours. Our calculations in Section 4 suggest that UV line blanketing could produce a redder spectrum (see Fig. 5). However, the value of $f \sim 5 \times 10^{-3}$ they nominally require is three orders of magnitude

higher than we predict from radioactive decay (Section 3.2.4). It thus appears more likely that the emission detected by Berger et al. is afterglow related (with the observed reddening perhaps due to dust).

Perhaps the most promising candidate kilonova detection to date was following GRB 080503, which showed an unusual rise in its optical afterglow light curve at $t \sim 1$ d before rapidly fading over the next several days (Perley et al. 2009). Although limited colour information was obtained near the emission peak, the observed light-curve evolution is largely consistent with that expected from a kilonova for an assumed ejecta velocity $v \sim 0.1c$ and mass $M_{\rm ej} \sim$ few $\times\ 10^{-2}\,{\rm M}_\odot$. However, although the event was well localized on the sky, no obvious host galaxy was detected coincident with the burst, despite the fact that a relatively low redshift $z \sim 0.1$ would be required to fit the observed peak brightness (if the event was indeed a kilonova). In principle, NS–NS/NS–BH binaries can receive natal 'kicks' from their supernovae which may eject them into intergalactic space, thereby making it difficult to identify their original host galaxy. This possibility is consistent with the very low density of the circumburst medium inferred for 080503. Perhaps more problematic for the kilonova interpretation, however, is the X-ray detection by *Chandra* coincident with the optical rise, which suggests that the optical emission at $\sim$1 d may simply be due to an (albeit unusual) non-thermal afterglow. The fact that the X-ray luminosity exceeds the optical luminosity appears especially difficult to explain if both are related to radioactively powered quasi-thermal emission.

Although the possible presence of kilonovae following short GRBs is not well constrained at present, this situation could in principle improve with additional sensitive, early-time optical/NIR observations of short GRBs. Indeed, *Swift* should remain operational through the next decade and presently detects short GRBs at a rate of about $\sim 10\,{\rm yr}^{-1}$. Unfortunately, however, this approach may encounter fundamental obstacles due to the non-thermal afterglow emission which also generally accompanies GRBs. In most accretion-powered GRB models, the luminosity of the burst increases with the accretion rate (e.g. McKinney 2005; Zalamea & Beloborodov 2009) and, hence, with the disc mass. Since the quantity of neutron-rich ejecta may be a relatively constant fraction of the disc mass (Metzger et al. 2009a; Section 2.1), the luminosity of the kilonova ($L_{\rm peak} \propto M_{\rm ej}^{1/2}$; equation 4) may positively correlate with the luminosity of the GRB.[3] Since the afterglow luminosities of short GRBs appear to scale with the prompt GRB fluence (as in long-duration GRBs; Nysewander, Fruchter & Pe'er 2009), the afterglow may generically swamp any putative kilonova emission. To date, this appears to be true even in cases when the circumburst density appears to be very low and the afterglow is relatively dim (Perley et al. 2009).

5.3 Blind optical transient surveys

In this section we assess the prospects for detecting kilonovae from NS–NS/NS–BH mergers with present and upcoming optical transient surveys. The virtue of such a search strategy is that it does not rely on a GW or high-energy EM trigger.

Based on observed binary NS systems, Kalogera et al. (2004) find that the NS–NS merger rate in the Milky Way is between 1.7×10^{-5} and $2.9 \times 10^{-4}\,{\rm yr}^{-1}$ at 95 per cent confidence. Population synthesis estimates (e.g. Belczynski et al. 2006) are consistent with this range but with larger uncertainties. Since there are no known BH–NS binaries, the BH–NS merger rate is even less certain. Bethe & Brown (1998) argue that BH–NS mergers could be substantially more common than NS–NS mergers, with Bethe, Brown & Lee (2007) estimating a rate $\sim 10^4\,{\rm Gpc}^{-3}\,{\rm yr}^{-1}$, corresponding to $\sim 10^{-3}\,{\rm yr}^{-1}$ in the Milky Way. An interesting limit can be placed on the total amount of neutron-rich ejecta from NS–NS/NS–BH merger from Galactic chemical evolution (e.g. Metzger et al. 2009a). Accounting for the total observed abundances of elements with $A \gtrsim 100$ in our Galaxy, for example, requires an average production rate $\sim 10^{-6}\,{\rm M}_\odot\,{\rm yr}^{-1}$ (e.g. Qian 2000). Assuming that a merger ejects $M_{\rm ej} \sim 10^{-2}\ (10^{-3})\,{\rm M}_\odot$ on average, the Galactic merger rate cannot exceed $\sim 10^{-4}\ (10^{-3})\,{\rm yr}^{-1}$ in order to avoid overproducing these rare neutron-rich isotopes (see further discussion in Section 5.3.1).

Assuming that the NS–NS rate is proportional to the blue stellar luminosity (Phinney 1991; Kopparapu et al. 2008), a Galactic rate of $R_{\rm NS-NS} \equiv 10^{-4} R_{-4}\,{\rm yr}^{-1}$ corresponds to a volumetric rate of $10^{-6} R_{-4}\,{\rm Mpc}^{-3}\,{\rm yr}^{-1}$. For $v = 0.1c$ and $M_{\rm ej} \sim 10^{-2} M_{\rm ej,-2}\,{\rm M}_\odot$ our calculations predict an optical transient with a peak V-band luminosity $\nu L_\nu \sim 3 \times 10^{41} M_{\rm ej,-2}^{1/2}\,{\rm erg\,s}^{-1}$ (Figs 5 and 6). For a limiting magnitude $M_V = 25(24)[21]$, this corresponds to a maximum detection (luminosity) distance of $D_{\rm L} = 1070(680)[170] M_{\rm ej,-2}^{1/4}\,{\rm Mpc}$ and a comoving volume $V = 2.8(0.9)[2 \times 10^{-2}]\ M_{\rm ej,-2}^{3/4}\,{\rm Gpc}^3$. The PTF 5-d cadence survey (Law et al. 2009), which surveys an active area $\sim 2700\,{\rm deg}^2$ to a limiting AB magnitude of 21, should therefore detect $\sim 1.4 R_{-4}\ M_{\rm ej,-2}^{3/4}\,{\rm yr}^{-1}$. Thus, if NS–NS mergers occur at the upper end of present rate estimates ($\sim 10^{-4}\,{\rm yr}^{-1}$) and $M_{\rm ej} \approx 10^{-2}\,{\rm M}_\odot$ is indeed representative, current surveys such as PTF should 'blindly' detect $\sim$1 merger yr^{-1}. We emphasize, however, that the total predicted rate of events and their luminosity function is sensitive to the distribution of ejecta masses $M_{\rm ej}$, which in principle could range from $\sim$0 to $0.1\,{\rm M}_\odot$ given present uncertainties (Section 2.1).

Prospects for detection are much better with the LSST, which will image the entire sky down to a limiting magnitude $\sim$24.5 every three–four nights and should detect NS–NS merger events at a rate $\sim 2 \times 10^3 R_{-4} M_{\rm ej,-2}^{3/4}\,{\rm yr}^{-1}$. Note that LSST is expected to come online in 2015, roughly coincident with Advanced LIGO/Virgo, and together they have the potential to completely revolutionize our understanding of compact object mergers.

Other thermal transients are predicted to occur in Nature on $\sim$day time-scales, which could be confused with NS–NS/NS–BH mergers. Examples include Type 'Ia' SNe due to unstable thermonuclear He flashes from white dwarf binaries (Bildsten et al. 2007; Poznanski et al. 2010) and Nickel-rich outflows from the accretion-induced collapse of white dwarfs (Metzger, Piro & Quataert 2009b; Darbha et al. 2010). Such events may originate from a similar stellar population to NS–NS/NS–BH mergers. However, one 'smoking gun' feature of kilonovae from NS–NS/NS–BH mergers is the presence of optical absorption lines due to heavy neutron-rich elements (as in r-process enriched halo stars; e.g. Sneden et al. 2003), which may not be present in white dwarf systems (although some r-process nuclei may be produced in neutrino-heated winds in the case of AIC; e.g. Dessart et al. 2006). Thus, NS–NS/NS–BH mergers may be distinguishable from other transients with rapid, deep spectroscopic observations. We plan to explore more detailed calculations of these r-process spectral features in future work.

In reality, only limited information will initially be available to transient searches (e.g. photometric colours, at best). Thus, the reddening of kilonovae at times $\gtrsim t_{\rm peak}$ (Fig. 5), if indeed robust,

[3] An exception may occur in the case of BH–NS mergers, where in some cases large amounts of material can be ejected relative to the mass of the accretion disc that forms (Rosswog 2005).

may be crucial for identifying these events. In fact, of the variable sources from the Sloan Digital Sky Survey characterized by Sesar et al. (2007), only a small fraction are as red as we predict kilonovae from NS–NS/NS–BH mergers to be at peak light ($U - V \gtrsim 2$ following peak brightness; compare our results in Fig. 5 with fig. 4 of Sesar et al. 2007). This suggests that a promising search strategy for detecting kilonovae is to trigger on anomalously red events of duration ∼thinsp;hour–day for more detailed follow-up observations.

5.3.1 *Implications for the origin of r-process elements*

The astrophysical origin of the *r*-process elements remains one of the great mysteries in nuclear astrophysics (see Qian & Wasserburg 2007 for a recent review), with the two chief candidates being core-collapse supernovae (e.g. Meyer et al. 1992) and NS–NS/NS–BH mergers (Freiburghaus et al. 1999; see Fig. 2). Since the luminosity of merger transients is directly related to their nucleosynthetic yield (equation 4), this implies that the detection of, or constraints on the rate of, kilonovae from NS mergers directly probes the origin of *r*-process elements.

As a concrete example, if one assumes that NS mergers are the dominant source of *r*-process elements in our Galaxy, then the mean mass ejected per event $\bar{M}_{\rm ej}$ and merger rate $\dot{N}_{\rm merge}$ are related by $\dot{N}_{\rm merge} = 10^{-4}\,{\rm yr}^{-1}(\bar{M}_{\rm ej}/10^{-2}\,{\rm M}_\odot)^{-1}$, where we have assumed a Galactic *r*-process production rate of $10^{-6}\,{\rm M}_\odot\,{\rm yr}^{-1}$ (e.g. Qian 2000). Since the kilonova luminosity $L_{\rm peak} \propto M_{\rm ej}^{1/2}$, the rate of detected transients $\propto L^{3/2}\dot{N}_{\rm merge} \propto \bar{M}_{\rm ej}^{-1/4} \propto \dot{N}_{\rm merge}^{1/4}$. Fig. 7 shows the expected detection rates versus $\dot{N}_{\rm merge}$ (or, equivalently, $\bar{M}_{\rm ej}$) with present and upcoming transient surveys if one assumes that NS–NS/NS–BH mergers are the dominant *r*-process source. Note that within the current uncertainties in $\dot{N}_{\rm merge}$, *current transient surveys should detect a few events per year if mergers are indeed the dominant source of the r-process*, independent of $\bar{M}_{\rm ej}$. In reality, the detection efficiency for low $\bar{M}_{\rm ej}$ may be somewhat lower than this simple estimate due to the shorter transient duration $t_{\rm peak} \propto M_{\rm ej}^{1/2}$ (equation 3).

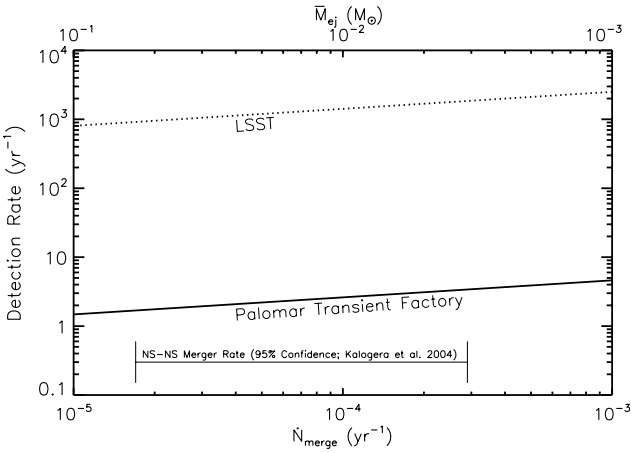

Figure 7. Rates of detected kilonovae from NS–NS/NS–BH mergers with present and upcoming surveys as a function of the merger rate $\dot{N}_{\rm merge}$ (bottom axis) or the average ejecta mass $\bar{M}_{\rm ej}$ (top axis), calculated under the assumption that NS–NS/NS–BH mergers are the primary source of *r*-process elements in the Galaxy. Also shown are the NS–NS merger rate estimates (95 per cent confidence interval) from Kalogera et al. (2004).

6 CONCLUSIONS

In their seminal paper on nucleosynthesis, Burbidge et al. (1957, B^{2}FH) proposed that SNe are powered by the radioactive decay of ^{254}Cf (cf. Burbidge et al. 1956). Although we now appreciate that most supernovae are powered by ^{56}Ni and ^{56}Co, the B^{2}FH picture of '*r*-process-powered' SNe still holds relevance for the neutron-rich ejecta from NS–NS/NS–BH mergers.

In this paper we have presented the first calculations of the radioactively powered transients from NS–NS/NS–BH mergers that self-consistently determine the radioactive heating using a nuclear reaction network and which accurately model the light curve and colour evolution with a radiative transfer calculation. Our main conclusions are summarized as follows.

(i) The radioactive heating $\dot{E}$ on time-scales $t_{\rm peak} \sim$ hours–days results (in approximately equal parts) from the fission and β-decays of heavy nuclei, which are produced by the *r*-process at much earlier times ($t \lesssim 1$ s; see Fig. 1). Our results for $\dot{E}$ at $t \sim t_{\rm peak}$ are relatively insensitive to the precise electron fraction and early-time expansion of the ejecta (e.g. whether it is dynamically ejected or wind driven), and to details of uncertain nuclear physics such as the theoretical nuclear mass model.

(ii) The net heating rate decreases approximately as a power law $\dot{Q} \propto t^{-\alpha}$ with $\alpha \sim 1.1$–1.4 for $t \sim$ hours–days, similar to the assumption $\dot{Q} \propto t^{-1}$ in the LP98 model. The total heating rate is $\sim 3 \times 10^{10}\,{\rm erg\,s^{-1}\,g^{-1}}$ at $t \approx 1$ d. By calibrating the LP98 model using our results, we find an effective 'f' parameter $\sim 3 \times 10^{-6}$ which is generally much lower than previously assumed.

(iii) β-decay electrons (Section 3.2.1) and fission daughter nuclei (Section 3.2.2) both thermalize with the plasma on time-scales $\sim t_{\rm peak}$, while only a portion of the γ-rays likely thermalize. We estimate that the *net* thermalization efficiency is $\epsilon_{\rm therm} \sim 0.5$–$1$ (Section 3.2).

(iv) For an ejecta mass $M_{\rm ej} \sim 10^{-2}$ to $10^{-3}\,{\rm M}_\odot$ we predict a transient that peaks on a time-scale $\sim$1 d at a bolometric and *V*-band luminosity $\sim 10^{42}\,{\rm erg\,s^{-1}}$ ($M_{\rm B} = -16$) and $\sim 3 \times 10^{41}\,{\rm erg\,s^{-1}}$ ($M_V = -15$), respectively (Figs 4 and 5).

(v) We argue that the transition metal *r*-process elements are likely to have UV absorption due to line blanketing (like Fe peak nuclei). As a result, we predict that NS merger transients will be relatively red (and redden in time; see Figs 5 and 6), a prediction not captured by assuming single-temperature blackbody emission. More detailed models of the colour evolution of NS merger transients will require a better understanding of the UV and IR spectral lines of second and third *r*-process peak elements (Section 4.1). The presence of absorption lines due to heavy *r*-process elements is one 'smoking gun' prediction of NS merger transients.

(vi) Because NS merger transients are isotropic, they can in principle be detected in three independent ways: in coincidence with a detected GW source; following a short-duration GRB and with blind optical/NIR transient surveys.

(vii) Given the low luminosities and rapid evolution of kilonovae from NS mergers, their detection will require close collaboration between the GW and astronomical communities. Given the unique observational signature of kilonovae, the real-time follow-up of GW detections with sensitive, wide-field telescopes could improve the effective sensitivity of LIGO/Virgo.

(viii) For an average ejecta mass $\bar{M}_{\rm ej} \approx 10^{-2}\,{\rm M}_\odot$, current surveys such as PTF should 'blindly' detect ∼ one NS merger transient per year if the merger rates lies at the high end of present estimates; LSST should detect $\sim 1000\,{\rm yr}^{-1}$ under the same assumptions.

(ix) Since the luminosity and detection rate of NS merger transients is closely related to the yield of heavy neutron-rich elements, *current* transient surveys are directly probing the unknown astrophysical origin of the *r*-process (Fig. 7). Holding the total *r*-process injection rate in the Milky Way fixed at $10^{-6}\,M_{\odot}\,yr^{-1}$ implies a detection rate $\sim$ few yr^{-1} and $\sim 10^{3}\,yr^{-1}$ for PTF and LSST, respectively, independent of the average ejecta mass.

ACKNOWLEDGMENTS

We thank G. Wahlgren, P. Shawhan, C. Sneden, F.-K. Thielemann and C. Blake for helpful conversations and useful information. We thank V. Petrosian for suggesting the term 'kilonovae' to describe NS merger transients. Support for BDM was provided by NASA through an Einstein Postdoctoral Fellowship grant number PF9-00065 awarded by the Chandra X-ray Center, which is operated by the Smithsonian Astrophysical Observatory for NASA under contract NAS8-03060. AA and GM-P are partly supported by the Deutsche Forschungsgemeinschaft through contract SFB 634 and the Helmholtz Alliance *Cosmic Matter in the Laboratory*. EQ was supported in part by the Miller Institute for Basic Research in Science, University of California Berkeley, and by the David and Lucile Packard Foundation. Support for DK was provided by NASA through Hubble fellowship grant #HST-HF-01208.01-A awarded by the Space Telescope Science Institute, which is operated by the Association of Universities for Research in Astronomy, Inc., for NASA, under contract NAS 5-26555. This research has been supported in part by the DOE SciDAC Program (DE-FC02-06ER41438). Support for RT and PN was provided by the Director, Office of Science, Office of High Energy Physics, of the US Department of Energy under Contract No. DE-AC02-05CH11231. IVP was supported in part by SCOPES project No. IZ73Z0-128180/1 awarded by the Swiss National Science Foundation, and by Russia Ministry of Education and Science, contract number 02.740.11.0250.

REFERENCES

Abbasi R. et al., 2009, Phys. Rev. Lett., 103, 221102
Abramovici A. et al., 1992, Sci, 256, 325
Arcones A., Janka H., Scheck L., 2007, A&A, 467, 1227
Arnett W. D., 1982, ApJ, 253, 785
Arun K. G. et al., 2009, Classical Quantum Gravity, 26, 094027
Baker J. G., Centrella J., Choi D.-I., Koppitz M., van Meter J., 2006, Phys. Rev. Lett., 96, 111102
Barzilay Y., Levinson A., 2008, New Astron., 13, 386
Becker A. C. et al., 2004, ApJ, 611, 418
Belczynski K., Perna R., Bulik T., Kalogera V., Ivanova N., Lamb D. Q., 2006, ApJ, 648, 1110
Benlliure J., Grewe A., de Jong M., Schmidt K.-H., Zhdanov S., 1998, Nuclear Phys. A, 628, 458
Berger E., 2009, ApJ, 690, 231
Berger E. et al., 2005, Nat, 438, 988
Berger E., Cenko S. B., Fox D. B., Cucchiara A., 2009, ApJ, 704, 877
Bethe H. A., Brown G. E., 1998, ApJ, 506, 780
Bethe H. A., Brown G. E., Lee C., 2007, Phys. Rep., 442, 5
Biémont É., Blagoev K., Fivet V., Malcheva G., Mayo R., Ortiz M., Quinet P., 2007, MNRAS, 380, 1581
Bildsten L., Shen K. J., Weinberg N. N., Nelemans G., 2007, ApJ, 662, L95
Bloom J. S. et al., 2006, ApJ, 638, 354
Bloom J. S. et al., 2009a, preprint (arXiv:0902.1527)
Bloom J. S. et al., 2009b, preprint (arXiv:0905.1965)
Burbidge G. R., Hoyle F., Burbidge E. M., Christy R. F., Fowler W. A., 1956, Phys. Rev., 103, 1145
Burbidge E. M., Burbidge G. R., Fowler W. A., Hoyle F., 1957, Rev. Modern Phys., 29, 547
Campanelli M., Lousto C. O., Marronetti P., Zlochower Y., 2006, Phys. Rev. Lett., 96, 111101
Caron B. et al., 1999, Astropart. Phys., 10, 369
Cayrel R., 1996, A&AR, 7, 217
Colgate S. A., Petschek A. G., Kriese J. T., 1980, ApJ, 237, L81
Cottingham W. N., Greenwood D. A., 2001, An Introduction to Nuclear Physics. Cambridge Univ. Press, Cambridge
Cutler C., Thorne K. S., 2002, General Relativity and Quantum Cosmology, preprint (gr-qc/0204090)
da Cruz M. T. F., Chan Y., Larimer R.-M., Lesko K. T., Norman E. B., Stokstad R. G., Wietfeldt F. E., Žlimen I., 1992, Phys. Rev. C, 46, 1132
Dalal N., Holz D. E., Hughes S. A., Jain B., 2006, Phys. Rev. D, 74, 063006
Darbha S., Metzger B. D., Quataert E., Kasen D., Nugent P., Thomas R., 2010, preprint (arXiv:1005.1081)
Deffayet C., Menou K., 2007, ApJ, 668, L143
Dessart L., Burrows A., Ott C. D., Livne E., Yoon S., Langer N., 2006, ApJ, 644, 1063
Dessart L., Ott C. D., Burrows A., Rosswog S., Livne E., 2009, ApJ, 690, 1681
Duez M. D., 2009, preprint (arXiv:0912.3529)
Duez M. D., Foucart F., Kidder L. E., Ott C. D., Teukolsky S. A., 2009, preprint (arXiv:0912.3528)
Eichler D., Livio M., Piran T., Schramm D. N., 1989, Nat, 340, 126
Faber J., 2009, Classical Quantum Gravity, 26, 114004
Fisker J. L., Martínez-Pinedo G., Langanke K., 1999, European Phys. J. A, 5, 229
Freiburghaus C., Rosswog S., Thielemann F., 1999, ApJ, 525, L121
Gaimard J.-J., Schmidt K.-H., 1991, Nuclear Phys. A, 531, 709
Gehrels N. et al., 2004, ApJ, 611, 1005
Goriely S., Demetriou P., Janka H., Pearson J. M., Samyn M., 2005, Nuclear Phys. A, 758, 587
Haensel P., Zdunik J. L., 1990a, A&A, 227, 431
Haensel P., Zdunik J. L., 1990b, A&A, 229, 117
Hjorth J. et al., 2005, Nat, 437, 859
Hoffman R. D., Woosley S. E., Qian Y., 1997, ApJ, 482, 951
Holz D. E., Hughes S. A., 2005, ApJ, 629, 15
Huba J. D., 2007, NRL Plasma Formulary. Wexford College Press, Palm Springs, CA
Hughes S. A., Holz D. E., 2003, Classical Quantum Gravity, 20, 65
Hurley K. et al., 2005, Nat, 434, 1098
Kaiser N. et al., 2002, in Tyson J. A., Wolff S., eds, Proc. SPIE Conf. Ser. Vol. 4836, Survey and Other Telescope Technologies and Discoveries. SPIE, Bellingham, p. 154
Kalogera V. et al., 2004, ApJ, 601, L179
Kalogera V., Belczynski K., Kim C., O'Shaughnessy R., Willems B., 2007, Phys. Rep., 442, 75
Kann D. A. et al., 2008, preprint (arXiv:0804.1959)
Kanner J., Huard T. L., Márka S., Murphy D. C., Piscionere J., Reed M., Shawhan P., 2008, Classical Quantum Gravity, 25, 184034
Kasen D., Woosley S. E., 2009, ApJ, 703, 2205
Kasen D., Thomas R. C., Nugent P., 2006, ApJ, 651, 366
Keller S. C. et al., 2007, Publ. Astron. Soc. Australia, 24, 1
Kim C., Kalogera V., Lorimer D. R., Ihm M., Belczynski K., 2005, in Rasio F. A., Stairs I. H., eds, ASP Conf. Ser. Vol. 328, Binary Radio Pulsars. Astron. Soc. Pac., San Francisco, p. 83
Kocevski D. et al., 2010, MNRAS, 404, 963
Kochanek C. S., Piran T., 1993, ApJ, 417, L17
Kopparapu R. K., Hanna C., Kalogera V., O'Shaughnessy R., González G., Brady P. R., Fairhurst S., 2008, ApJ, 675, 1459
Kowalski M., Mohr A., 2007, Astropart. Phys., 27, 533
Krolak A., Schutz B. F., 1987, Gen. Relativ. Gravitation, 19, 1163
Kulkarni S. R., 2005, preprint (astro-ph/0510256)
Kurucz R. L., Bell B., 1995, Atomic Line List, Kurucz CD-ROM. Smithsonian Astrophys. Obs., Cambridge, MA
Lattimer J. M., Schramm D. N., 1974, ApJ, 192, L145
Lattimer J. M., Schramm D. N., 1976, ApJ, 210, 549

Law N. M. et al., 2009, PASP, 121, 1395
Lawler J. E., Den Hartog E. A., Sneden C., Cowan J. J., 2006, ApJS, 162, 227
Lawler J. E., den Hartog E. A., Labby Z. E., Sneden C., Cowan J. J., Ivans I. I., 2007, ApJS, 169, 120
Lawler J. E., Sneden C., Cowan J. J., Ivans I. I., Den Hartog E. A., 2009, ApJS, 182, 51
Lee W. H., Ramirez-Ruiz E., López-Cámara D., 2009, ApJ, 699, L93
Li L., Paczyński B., 1998, ApJ, 507, L59 (LP98)
LIGO Scientific Collaboration, Virgo Collaboration, 2010, preprint (arXiv:1003.2480)
McKinney J. C., 2005, ApJ, 630, L5
Mancini D. et al., 2000, in Sebring T. A., Andersen T., eds, Proc. SPIE Conf. Ser. Vol. 4004, Telescope Structures, Enclosures, Controls, Assembly/Integration/Validation, and Commissioning. SPIE, Bellingham, p. 79
Márka S., Mours B., Williams R., 2002, Classical Quantum Gravity, 19, 1537
Martínez-Pinedo G., 2008, European Phys. J. – Special Topics, 156, 123
Martínez-Pinedo G. et al., 2007, Progress Part. Nuclear Phys., 59, 199
Metzger B. D., Quataert E., Thompson T. A., 2008a, MNRAS, 385, 1455
Metzger B. D., Piro A. L., Quataert E., 2008b, MNRAS, 390, 781
Metzger B. D., Thompson T. A., Quataert E., 2008c, ApJ, 676, 1130
Metzger B. D., Piro A. L., Quataert E., 2009a, MNRAS, 396, 304
Metzger B. D., Piro A. L., Quataert E., 2009b, MNRAS, 396, 1659
Metzger B. D., Arcones A., Quataert E., Martínez-Pinedo G., 2010, MNRAS, 402, 2771
Meyer B. S., 1989, ApJ, 343, 254
Meyer B. S., Mathews G. J., Howard W. M., Woosley S. E., Hoffman R. D., 1992, ApJ, 399, 656
Möller P., Nix J. R., Myers W. D., Swiatecki W. J., 1995, Atomic Data Nuclear Data Tables, 59, 185
Möller P., Pfeiffer B., Kratz K.-L., 2003, Phys. Rev. C, 67, 055802
Nakar E., Gal-Yam A., Fox D. B., 2006, ApJ, 650, 281
Narayan R., Paczynski B., Piran T., 1992, ApJ, 395, L83
Nysewander M., Fruchter A. S., Pe'er A., 2009, ApJ, 701, 824
Paczynski B., 1986, ApJ, 308, L43
Padmanabhan T., 2000, Theoretical Astrophysics, Vol. 1, Astrophysical Processes. Cambridge Univ. Press, Cambridge
Panov I. V., Korneev I. Y., Rauscher T., Martínez-Pinedo G., Kelić-Heil A., Zinner N. T., Thielemann F.-K., 2010, A&A, 513, A61
Pearson J. M., Nayak R. C., Goriely S., 1996, Phys. Lett. B, 387, 455
Perley D. A. et al., 2009, ApJ, 696, 1871
Petermann I. et al., 2008, in Proc. 10th Symp. Nuclei in the Cosmos (NIC X). Proc. Sci., Trieste, p. 143
Phinney E. S., 1991, ApJ, 380, L17
Phinney E. S., 2009, in Blandford R. et al. eds, Astro2010 Decadal Survey. Nat. Acad. Sci., Washington, DC, p. 235
Pinto P. A., Eastman R. G., 2000, ApJ, 530, 757
Poznanski D. et al., 2010, Sci, 327, 58
Pretorius F., 2005, Phys. Rev. Lett., 95, 121101
Qian Y., 2000, ApJ, 534, L67
Qian Y., Wasserburg G. J., 2007, Phys. Rep., 442, 237
Rau A. et al., 2009, PASP, 121, 1334
Rauscher T., Thielemann F.-K., 2000, Atomic Data Nuclear Data Tables, 75, 1
Rhoads J. E., 1999, ApJ, 525, 737
Rossi E. M., Perna R., Daigne F., 2008, MNRAS, 390, 675
Rosswog S., 2005, ApJ, 634, 1202
Rosswog S., Liebendörfer M., Thielemann F., Davies M. B., Benz W., Piran T., 1999, A&A, 341, 499
Ruffert M., Janka H., Takahashi K., Schaefer G., 1997, A&A, 319, 122
Schutz B. F., 1986, Nat, 323, 310
Schutz B. F., 2002, in Gilfanov M., Sunyeav R., Churazov E., eds, ESO Astrophys. Symp. Proc. XIV, Lighthouses of the Universe: The Most Luminous Celestial Objects and Their Use for Cosmology. Springer, Berlin, p. 207
Sesar B. et al., 2007, AJ, 134, 2236
Sneden C. et al., 2003, ApJ, 591, 936
Soderberg A. M., Nakar E., Berger E., Kulkarni S. R., 2006a, ApJ, 638, 930
Soderberg A. M. et al., 2006b, ApJ, 650, 261
Stamatikos M., Gehrels N., Halzen F., Mészáros P., Roming P. W. A., 2009, in Blandford R. et al. eds, Astro2010 Decadal Survey. Nat. Acad. Sci., Washington, DC, p. 284
Strauss M. A. et al., 2010, American Astron. Soc. Meeting Abstr., 215, 401.01
Stubbs C. W., 2008, Classical Quantum Gravity, 25, 184033
Surman R., McLaughlin G. C., Ruffert M., Janka H., Hix W. R., 2008, ApJ, 679, L117
Swartz D. A., Sutherland P. G., Harkness R. P., 1995, ApJ, 446, 766
Sylvestre J., 2003, ApJ, 591, 1152
Timmes F. X., Arnett D., 1999, ApJS, 125, 277
Totani T., Panaitescu A., 2002, ApJ, 576, 120
Villasenor J. S. et al., 2005, Nat, 437, 855
Zalamea I., Beloborodov A. M., 2009, in Meegan C., Kouveliotou C., Gehrels N., eds, AIP Conf. Ser. Vol. 1133, Gamma-Ray Burst: Sixth Huntsville Symposium. Am. Inst. Phys., New York, p. 121
Zhang W., MacFadyen A., 2009, ApJ, 698, 1261

This paper has been typeset from a TEX/LATEX file prepared by the author.